

# SMAP: Simultaneous Mapping and Planning on Occupancy Grids

1

Ali-akbar Agha-mohammadi

## Abstract

Occupancy grids are the most common framework when it comes to creating a map of the environment using a robot. This paper studies occupancy grids from a planning perspective and proposes a mapping method that provides richer data (map) for the purpose of planning and collision avoidance. Typically, in occupancy grid mapping, each cell contains a single number representing the probability of cell being occupied. In the proposed planning-oriented representation, we maintain a probability distribution over this number, which allows the planner to reason about acquisition of the future observation. The planning with this confidence-aware map, leads to active perception maneuvers that while guiding the robot toward the goal aims at increasing the confidence in parts of the map that are relevant to accomplishing the task.

## I. INTRODUCTION

Consider a Quadrotor flying in an obstacle-laden environment, tasked to reach a goal point while mapping the environment with a forward-facing stereo camera. To carry out the sense-and-avoid task, and ensure the safety of the system by avoiding collisions, the robot needs to create a representation of obstacles, referred to as the map, and incorporate it in the planning framework. This paper is concerned with the design of such a framework where there is tight integration between mapping and planning. The main advantage of such tight integration and joint design of these two blocks is that not only mapping can provide the information for the planning (or navigation) module, but also the navigation module can generate maneuvers that lead to better mapping and more accurate environment representation.

*Generic frameworks to solve this problem:* Grid-based structures are among the most common representation of the environment when dealing with the stereo cameras. Typically, each grid voxel contains a boolean information that if the cell is free or occupied by obstacles. Or in a richer format each voxel contains the probability of the cell being occupied. Traditionally such representation is generated assuming that the robot actions are given based on some map-independent cost. However, in a joint design of planning and mapping, one *objective* of planning could be the accuracy of generated map.

*Contributions and highlights:* Characterizing a map accuracy and how it is affected by the output of the planner is the first challenge in such a joint design. The contributions of this work can be listed as follows:

- 1) We propose a novel planning framework where active perception/mapping is accomplished via incorporating mapping accuracy into the planning.
- 2) We propose a mapping framework whose future evolution under planner actions can be predicted accurately.
- 3) The proposed method is capable of coping with maps where each voxel might be partially occupied by obstacles.

*Paper organization:* We start by the problem statement and a review of the log-odds based mapping method in the next two sections. In section IV, we discuss the sensor model we consider for the stereo camera. Section V describes our mapping framework. In Section VI, we explain the planning algorithm. Section VII demonstrate the results of the proposed mapping method in a simulated scenario.

## II. PROBLEM STATEMENT

**Density map:** Let  $G = [G^1, \dots, G^M]$  be a grid overlaid on the 3D environment, where  $G^i \in \mathbb{R}^3$  is a 3D point representing the center of the  $i$ -th voxel of the grid. Density map  $m = [m^1, \dots, m^M]$  is defined as a set of values over this grid, where  $m^i \in [0, 1]$  represents the density of environment obstacles falling under the  $i$ -th voxel of the grid. For example  $m^i = .3$  if the 30 percent of the  $i$ -th voxel is occupied by obstacles. In this paper, we use words density and “occupancy level” interchangeably. The special case of density maps are occupancy grid maps where  $m^i \in \{0, 1\}$ , which is a good approximation of density when voxels are small [1]. We overload the variable  $m^i$  with function  $m^i[x]$  that returns the 3D location of the  $i$ -th voxel in the global coordinate frame.

**Map belief:** Obtaining measurements via a noisy sensor, the best one can hope for is to have an estimate of the density values, rather than their exact values. We denote the sensor measurement at the  $k$ -th time step by  $z_k$  and the sensor configuration at the  $k$ -th time step with  $xv_k$ . Formulating the problem in a Bayesian framework, we compress the information obtained from past measurements  $z_{0:k} = \{z_0, \dots, z_k\}$  and  $xv_{0:k} = \{xv_0, \dots, xv_k\}$  to create a probability distribution  $b_k^m$  on all possible values of density.

$$b_k^m = p(m|z_{0:k}, xv_{0:k}) \quad (1)$$

The goal of this paper is three fold: Derive 1) density-based ranging sensor model, 2) recursive density mapping, and 3) map-enhancing motion planning scheme.

- 1) **Density-based ranging sensor model:** First, given the obstacles are described by a density grid, we would like to create a ranging sensor model (mainly for stereo camera), i.e., derive the probability of getting measurement  $z$  given a stochastic density map and robot location.

$$p(z_k|xv_k, b_k^m) \quad (2)$$

- 2) **Recursive density mapping:** We would like to derive a recursive mapping scheme  $\tau$  that updates the current density map based on the last measurements

$$b_{k+1}^m = \tau^m(b_k^m, z_{k+1}, xv_{k+1}) \quad (3)$$

- 3) **Motion planning and active perception in density maps:** Finally, we would like to design a planning scheme that moves the robot from start to goal, while incorporating density map and taking actions that actively reducing uncertainty on the map to generate safer paths with lower collision probabilities.

$$\pi^* = \arg \min_{\Pi} J(x_k, b_k^m, \pi) \quad (4)$$

We will discuss these three goals in the next three sections.

## III. TRADITIONAL OCCUPANCY GRID MAPPING

In this section, we briefly review the most common occupancy grid mapping method in robotics research literature and discuss some of differences with the proposed method in this paper.

**Assumption 1. Cell independence:** *It is assumed that occupancy of voxels are independent given the measurement history. Mathematically, for voxels  $i$  and  $j$ , we have:*

$$p(m^i, m^j|z_{0:k}, xv_{0:k}) \approx p(m^i|z_{0:k}, xv_{0:k})p(m^j|z_{0:k}, xv_{0:k}) \quad (5)$$

However, much stronger assumption is:

**Assumption 2. Measurement independence:** *It is assumed that occupancy of voxels are independent given the measurement history. Mathematically, for voxels  $i$  and  $j$ , we have:*

$$p(z_k|m^i, z_{0:k-1}, xv_{0:k}) \approx p(z_k|m^i, xv_k) \quad (6)$$

Note that Assumption 2 would be precise if conditioning is over the whole map. In other words,

$$p(z_k|m, z_{0:k-1}, xv_{0:k}) = p(z_k|m, xv_k) \quad (7)$$

is correct. But, when conditioning on a single voxel, the independence does not hold.

**Relaxing assumptions:** In this paper, we relax Assumption 2 and use a slightly weaker version of Assumption 1.

#### IV. DEPTH-SENSOR MODELING

In this section, we model a range sensor when the environment representation is a density map.

**Disparity sensor:** In this paper, we focus on a stereo camera, but results are generalizable to other range sensors as well. Stereo camera is a passive sensor where comparing the image from left and right cameras can be translated to a disparity image, which in turn can be converted to the depth. Let us denote the camera center by  $x$  and the 3D location of the  $i$ -th pixel by  $v$ . We denote the ray emanating from  $x$  and passing through  $v$  by  $xv = (x, v)$ . Denoting the distance of the closest obstacle from the camera along ray  $xv$  by  $r$ , the disparity  $z$  of this pixel, in the absence of noise, is:

$$z = r^{-1} f d_b \quad (8)$$

where,  $f$  is camera's focal length and  $d_b$  is the baseline between two cameras on the stereo rig. In this paper we abstract the stereo sensor model to the hypothetical "disparity sensor" model. Also, we treat each pixel as a separate sensor and focus on deriving the disparity sensor model for the single pixel  $v$ , i.e.,  $z = h(xv, b^m)$  or equivalently represented by its likelihood  $p(z|xv, b^m)$ .

**Pixel cone:** Consider the narrow 3D cone with apex at  $x$  and boundaries defined by pixel  $v$  (this cone can be approximated by the ray  $xv$  going through point  $x$  and center of pixel  $v$ .) Pixel cone  $\text{Cone}(xv)$  refers to the set of voxels in map  $m$  that falls into the mentioned narrow cone (or approximately set of voxels that intersects with ray  $xv$ .) We denote this set by  $\mathbb{C} = \text{Cone}(xv)$ , where  $\mathbb{C} \subset m$ .

**Cause variables:** The disparity measurement on pixel  $v$  could be the result of light reflection from any of voxels in the cone  $\mathbb{C} = \text{Cone}(xv)$  (see Fig. 1). Therefore any of these voxels is a potential cause for the measurement. In the case that the environment map is perfectly known, one can pinpoint the exact cause by finding the closest obstacle to the camera center. But, when the knowledge about the environment is partial and probabilistic, the best one can deduce about causes is a probability distribution over all possible causes in the pixel cone  $\mathbb{C} = \text{Cone}(xv)$ . These causes will play an important role (as hidden variables) in deriving sensor model for stochastic maps.

**Local vs global indices:** For a given ray  $xv$ , we can order the voxels along the ray from the closest to the camera to the farthest from the camera. Let  $l \in \{1, \dots, \|\mathbb{C}\|\}$  denote the local index of the voxel on ray  $xv$ . Then the function  $g = \gamma(l, xv)$  returns the global index  $g$  of this voxel in the map.

**Cause probability:** To derive the full sensor model, we need to reason about which voxel was the cause for a given measurement. For a voxel  $c \in \mathbb{C}(xv)$  to be cause, two events need to happen: (i) Event  $B^c$ , which indicates the event of light bouncing from the voxel and (ii) Event  $R^c$ , which indicates the event of light reaching the camera.

$$p(c|b^m) = \Pr(B^c, R^c|b^m) = \Pr(R^c|B^c, b^m) \Pr(B^c|b^m) \quad (9)$$

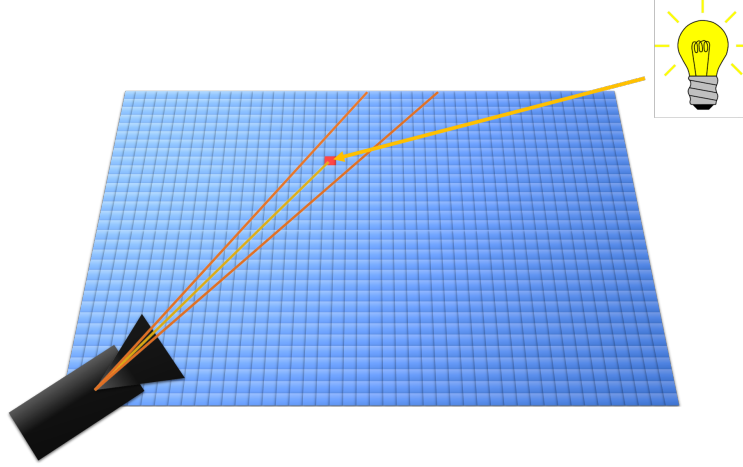


Fig. 1. Cone formed by two red lines denotes a code associated with a given pixel  $v$  on the image plane. The disparity measurement on pixel  $v$  can be affected by light coming from any of voxels in the pixel cone. In this figure, the measurement is created by the reflection from the "red" voxel.

**Bouncing probability:** To compute the bouncing probability, we rely on the fact that  $\Pr(B^c|m^c) = m^c$  by the definition of the density. In other words, the occupancy level of the voxel  $c$  is the probability of ray bouncing from that voxel. The assumption here is that the environment is texture-rich. Accordingly, we can write:

$$\begin{aligned}
 \Pr(B^c|b^m) &= \int_0^1 \Pr(B^c|m^c, b^m) p(m^c|b^m) dm^c \\
 &= \int_0^1 \Pr(B^c|m^c) p(m^c|b^m) dm^c \\
 &= \int_0^1 m^c b^m dm^c = \mathbb{E}m^c = \hat{m}^c
 \end{aligned} \tag{10}$$

**Reaching probability:** For the ray emanating from voxel  $c$  to reach the image plane, it has to go through all voxels on ray  $xv$  and not  $c$ . Let  $c^l$  denotes local index of voxel  $c$  along the ray  $xv$ , i.e.,  $c^l = g^{-1}(c, xv)$ , then we have:

$$\begin{aligned}
 \Pr(R^c|B^c, b^m) &= (1 - \Pr(B^{g(c^l-1, xv)}|b^m)) \Pr(R^{g(c^l-1, xv)}|B^{g(c^l-1, xv)}, b^m) \\
 &= \prod_{l=1}^{c^l-1} (1 - \Pr(B^{g(l, xv)}|b^m)) = \prod_{l=1}^{c^l-1} (1 - \hat{m}^{g(l, xv)})
 \end{aligned} \tag{11}$$

**Sensor model with known cause:** Assuming the cause voxel for measurement  $z$  is known, it is straightforward to design the sensor model.

$$z = h(xv, c, n_z) = \|G^c - x\|^{-1} f db + n_z, \quad n_z \sim \mathcal{N}(0, R) \tag{12}$$

where,  $n_z$  denotes the observation noise, which is modeled as a zero-mean Gaussian with variance  $R$ . We can alternatively describe the observation model in terms of pdfs as follows:

$$p(z|xv, c) = \mathcal{N}(\|G^c - x\|^{-1} f db, R) \tag{13}$$

**Senosr model with stochastic maps:** Sensor model given a stochastic map can be computed by incorporating hidden cause variables into the formulation:

$$p(z|xv; b^m) = \sum_{c \in \mathbb{C}(xv)} p(z|xv, c; b^m) \Pr(c|b^m) \quad (14)$$

$$= \sum_{c \in \mathbb{C}(xv)} \mathcal{N}(\|G^c - x\|^{-1} f d_b, R) \hat{m}^c \prod_{l=1}^{c^l-1} (1 - \hat{m}^{g(l, xv)}) \quad (15)$$

## V. CONFIDENCE-AUGMENTED GRID MAP

In this section, we derive the mapping algorithm that can reason not about the probability of collision at each cell, but also about the confidence level of this value. As a result, it enables efficient prediction of the map that can be embedded in planning and resulted in safer plans.

**assumption and approximations:** Small lemma: Given the cause, the last measurement is irrelevant:

$$\begin{aligned} p(m^i|c_k, z_{0:k}, xv_{0:k}) &= \frac{p(z_k|m^i, c_k, z_{0:k-1}, xv_{0:k})p(m^i|c_k, z_{0:k-1}, xv_{0:k})}{p(z_k|c_k, z_{0:k-1}, xv_{0:k})} \\ &= \frac{p(z_k|c_k, z_{0:k-1}, xv_{0:k})p(m^i|c_k, z_{0:k-1}, xv_{0:k})}{p(z_k|c_k, z_{0:k-1}, xv_{0:k})} \\ &= p(m^i|c_k, z_{0:k-1}, xv_{0:k}) \end{aligned} \quad (16)$$

**Bayesian update:** We start by  $p(m^i|z_{0:k}, xv_{0:k})$ , and using above lemma, we get:

$$\begin{aligned} p(m^i|z_{0:k}, xv_{0:k}) &= \sum_{c_k \in \mathbb{C}(xv)} p(m^i|c_k, z_{0:k}, xv_{0:k}) \Pr(c_k|z_{0:k}, xv_{0:k}) \\ &= \sum_{c_k \in \mathbb{C}(xv)} p(m^i|c_k, z_{0:k-1}, xv_{0:k}) \Pr(c_k|z_{0:k}, xv_{0:k}) \\ &= \sum_{c_k \in \mathbb{C}(xv)} \frac{\Pr(c_k|m^i, z_{0:k-1}, xv_{0:k})}{\Pr(c_k|z_{0:k-1}, xv_{0:k})} \Pr(c_k|z_{0:k}, xv_{0:k})p(m^i|z_{0:k-1}, xv_{0:k}) \\ &= \sum_{c_k \in \mathbb{C}(xv)} \frac{\Pr(c_k|m^i, z_{0:k-1}, xv_{0:k})}{\Pr(c_k|z_{0:k-1}, xv_{0:k})} \Pr(c_k|z_{0:k}, xv_{0:k})p(m^i|z_{0:k-1}, xv_{0:k-1}) \end{aligned} \quad (17)$$

**Compressions:** Then, we rely on below compression (based on sufficient statistics):

$$p(c_k, m^i|z_{0:k-1}, xv_{0:k-1}) = p(c_k, m^i|b_{k-1}^m) \quad (18)$$

$$\Pr(c_k|z_{0:k}, xv_{0:k}) = \Pr(c_k|b_{k-1}^m, z_k, xv_k) \quad (19)$$

**Bayesian update with map belief:** Now, we can re-write (17) as:

$$p(m^i|z_{0:k}, xv_{0:k}) = \sum_{c_k \in \mathbb{C}(xv)} \frac{\Pr(c_k|m^i, b_{k-1}^m, xv_k)}{\Pr(c_k|b_{k-1}^m, xv_k)} \Pr(c_k|b_{k-1}^m, z_k, xv_k)p(m^i|z_{0:k-1}, xv_{0:k-1}) \quad (20)$$

**Main approximation:** To see the approximation more clearly, one can replace  $b_{k-1}^m$  with  $(z_{0:k-1}, xv_{0:k-1})$ :

$$\Pr(B^{c_k} | m^i, b_{k-1}^m, xv_k) \approx \begin{cases} \hat{m}^{c_k} & \text{if } c_k \neq i \\ m^i & \text{if } c_k = i \end{cases}$$

Note that the second line (when  $c_k^l = i^l$ ) is exact, but the first line is an approximation. However, this is a tight approximation. Basically, the underlying assumption is: "the bouncing probability from voxel  $c$  when  $c \neq i$  is independent of voxel  $i$  given a stochastic map.

$$\mathbb{E}[m^{c_k} | m^i, z_{0:k-1}, xv_{0:k}] \approx \begin{cases} \mathbb{E}[m^{c_k} | z_{0:k-1}, xv_{0:k}] & \text{if } c_k \neq i \\ m^i & \text{if } c_k = i \end{cases}$$

In a more compact form

$$\Pr(B^{c_k} | m^i, b_{k-1}^m, xv_k) = \mathbb{E}[m^{c_k} | m^i, z_{0:k-1}, xv_{0:k}] \approx \mathbb{E}[m^{c_k} | z_{0:k-1}, xv_{0:k}] = \hat{m}^{c_k} \quad \text{for } c_k \neq i$$

**Cause ratio:** Let us focus on the ratio within (20), which describes the ratio between cause probability with and without conditioning on the true value of map at the  $i$ -th voxel. Dropping  $xv$  term to unclutter the equations, we can expand the numerator as:

$$\begin{aligned} p(c_k | m^i, b_{k-1}^m, xv_k) &= \Pr(B^{c_k}, R^{c_k} | m^i, b_{k-1}^m, xv_k) = \Pr(B^{c_k} | m^i, b_{k-1}^m, xv_k) \Pr(R^{c_k} | B^{c_k}, m^i, b_{k-1}^m, xv_k) \\ &\approx \begin{cases} \hat{m}^{c_k} \prod_{l=1}^{c_k^l-1} (1 - \hat{m}^{g(l, xv)}) & \text{if } c_k^l < i^l \\ m^i \prod_{l=1}^{c_k^l-1} (1 - \hat{m}^{g(l, xv)}) & \text{if } c_k^l = i^l \\ \hat{m}^{c_k} \left( \prod_{l=1}^{i^l-1} (1 - \hat{m}^{g(l, xv)}) \right) (1 - m^i) \left( \prod_{l=i^l+1}^{c_k^l-1} (1 - \hat{m}^{g(l, xv)}) \right) & \text{if } c_k^l > i^l \end{cases} \end{aligned} \quad (21)$$

whereas the denominator is  $p(c_k | b_{k-1}^m, xv_k) = \hat{m}^{c_k} \prod_{l=1}^{c_k^l-1} (1 - \hat{m}^{g(l, xv)})$  for all  $c_k \in \mathbb{C}(xv)$ . In these equations,  $c_k^l = g^{-1}(c_k, xv_k)$  and  $i^l = g^{-1}(i, xv_k)$  are the corresponding indices of  $c_k$  and  $i$  in the local frame.

According to the cause probability definitions, the ratio can be written as:

$$\frac{\Pr(c_k | m^i, b_{k-1}^m, xv_k)}{\Pr(c_k | b_{k-1}^m, xv_k)} = \begin{cases} 1 & \text{if } c_k^l < i^l \\ m^i (\hat{m}^i)^{-1} & \text{if } c_k^l = i^l \\ (1 - m^i) (1 - \hat{m}^i)^{-1} & \text{if } c_k^l > i^l \end{cases}$$

Plugging the ratio back into the (20), we get:

$$\begin{aligned} p(m^i | z_{0:k}, xv_{0:k}) &= \left[ \sum_{c_k^l=1}^{i^l-1} \Pr(c_k | b_{k-1}^m, z_k, xv_k) + m^i (\hat{m}^i)^{-1} \Pr(c_k | b_{k-1}^m, z_k, xv_k) \right. \\ &\quad \left. + (1 - m^i) (1 - \hat{m}^i)^{-1} \sum_{c_k^l=i^l+1}^{|\mathbb{C}(xv)|} \Pr(c_k | b_{k-1}^m, z_k, xv_k) \right] p(m^i | z_{0:k-1}, xv_{0:k-1}) \end{aligned} \quad (22)$$

Collecting linear and constant terms, we can simplify (22) as:

$$p(m^i | z_{0:k}, xv_{0:k}) = (\alpha^i m^i + \beta^i) p(m^i | z_{0:k-1}, xv_{0:k-1}) \quad (23)$$

where

$$\alpha^i = \sum_{c_k^l=1}^{i^l-1} \Pr(c_k|b_{k-1}^m, z_k, xv_k) + (1 - \hat{m}^i)^{-1} \sum_{c_k^l=i^l+1}^{|\mathbb{C}(xv)|} \Pr(c_k|b_{k-1}^m, z_k, xv_k) \quad (24)$$

$$\beta^i = (\hat{m}^i)^{-1} \Pr(c_k|b_{k-1}^m, z_k, xv_k) - (1 - \hat{m}^i)^{-1} \sum_{c_k^l=i^l+1}^{|\mathbb{C}(xv)|} \Pr(c_k|b_{k-1}^m, z_k, xv_k) \quad (25)$$

In a more compact form, one can rewrite equation (23) as:

$$b_{k+1}^{m^i} = \tau^i(b_k^{m^i}, z_{k+1}, xv_{k+1}) \quad (26)$$

where,  $b_k^{m^i} = p(m^i|z_{0:k}, xv_{0:k})$ .

**Inverse cause model:**

$$\begin{aligned} \Pr(c_k|z_{0:k}, xv_{0:k}) &= \Pr(c_k|b_{k-1}^m, z_k, xv_k) \\ &= \frac{p(z_k|c_k, xv_k) \Pr(c_k|b_{k-1}^m, xv_k)}{p(z_k|b_{k-1}^m, xv_k)} \\ &= \eta' p(z_k|c_k, xv_k) \Pr(c_k|b_{k-1}^m, xv_k) \\ &= \eta' p(z_k|c_k, xv_k) \hat{m}_{k-1}^{c_k} \prod_{j=1}^{c_k^l-1} (1 - \hat{m}_{k-1}^{g(j, xv)}), \quad \forall c_k \in \mathbb{C}(xv_k) \end{aligned} \quad (27)$$

## VI. PLANNING WITH CAG-MAP

In this section, we describe the planning method that utilizes the confidence-rich representation proposed in the previous section.

The objective in planning is to get to the goal point, while avoiding obstacles (e.g., minimizing collision probability). To accomplish this, the planner needs to reason about the acquisition of future perceptual knowledge and incorporate this knowledge in planning. An important feature of the confidence-right map is that it enables efficient prediction of the map evolution and map uncertainty.

**Future observations:** However, reasoning about future costs, one needs to first reason about future observations. The precise way of incorporating unknown future observations is to treat them as random variables and compute their future pdf. But, a common practice in belief space planning literature is to use the most likely future observations as the representative of the future observations to reason about the evolution of belief. Let us denote the most likely observation at the  $n$ -th step by:

$$z_n^{ml} = \arg \max_z p(z|b_n^m, xv_n) \quad (28)$$

**Future map beliefs:** Accordingly, we can compute most likely future map beliefs:

$$b_{n+1}^{m^i, ml} = \tau^i(b_n^{m^i, ml}, z_{n+1}^{ml}, xv_{n+1}), \quad n \geq k \quad (29)$$

where,  $b_k^{m^i, ml} = b_k^{m^i}$ .

**Path cost:** To assign a cost  $J(x_k, b_k^m, path)$  to a given path  $path = (xv_k, u_k, xv_{k+1}, u_{k+1}, \dots, xv_N)$  starting from  $xv_k$ , when map looks like  $b_k^m$ , one needs to predict the map belief along the path via (29). Assuming an additive cost we can get the path cost by adding up one-step costs:

$$J(x_k, b_k^m, path) = \sum_{n=k}^N c(b_n^{m, ml}, xv_n, u_n) \quad (30)$$

where the cost in belief space is induced by an underlying cost in the state space, i.e.,

$$c(b_n^{m,ml}, xv_n, u_n) = \int c(m_n, xv_n, u_n; b_n^{m,ml}) b_n^{m,ml}(m_n) dm_n \quad (31)$$

**One-step cost:** The underlying one-step cost  $c(m_n, xv_n, u_n; b_n^{m,ml})$  depends on the application in hand. For safe navigation with grid maps, we use the following cost function:

$$c(m, xv, u; b^m) = m^j + (m^j - \hat{m}^j)^2 \quad (32)$$

where,  $j$  is the index of the cell, the robot is at. In other words,  $x \in m^j$ .

As a result the cost in belief space will be:

$$c(b_n^m, xv_n, u_n) = \hat{m}_n^j + \sigma(m_n^j) = \mathbb{E}[m_n^j | z_{k+1:n}, xv_{k+1:n}, b_k^m] + \text{Var}[m_n^j | z_{k+1:n}, xv_{k+1:n}, b_k^m] \quad (33)$$

above observations are "future observation".

**Path planning:** To generate the plan we use the RRT method [2] to create a set of candidate trajectories  $\Pi = \{path^i\}$ . For each trajectory, we compute the cost  $c(path^i)$  and pick the path with minimum cost.

$$path^* = \arg \min_{\Pi} J(x_k, b_k^m, path) \quad (34)$$

## VII. SIMULATION RESULTS: OCCUPANCY GRID MAPPING

In this section, we compare the map resulted from the proposed mapping method with traditional log-odds based grid mapping. The ground truth map is shown in Fig. 2. Each voxel is assumed to be a square with 10cm side length. The environment size is 2m-by-2m, consists of 400 voxels. Each voxel is either fully occupied (shown in black) or empty (white). We randomly populate the voxels by 0 and 1's, except the voxels in the vicinity of the robot, which are set to be free. The robot's x-y position is static and set to (0, 0). The robot orientation is changing with a fixed angular velocity of 15 degrees per second. We run simulations for 50 seconds, almost equivalent to two full turns.

For the sensing system, we have simulated a simple stereo camera in 2D. The range of sensor is 1 meter, with a field of view of 28 degrees. There are 15 pixels along the simulated image plane. The field of view is shown in Fig. 2 as a red cone. Measurement frequency is 10Hz. The measurement noise is assumed to be a zero-mean Gaussian with variance 0.04.

For the log-odds mapping, we use a typical inverse sensor model as seen in Fig. 3. One of the best results we have got from log-odds mapping is obtained by setting the inverse sensor parameters to:  $r_{ramp} = 0.1$ ,  $r_{top} = 0.1$ ,  $q_l = 0.45$ , and  $q_h = 0.55$ .

The map resulted from log-odds method (using the above inverse sensor model) and from the proposed method are shown in Fig. 4 and 5, respectively. Note that while the inverse sensor model needs to be tuned for the log-odds-based mapping, in the proposed mapping methods, there are no parameters for tuning.

To quantify the difference between the maps resulted from the log-odds and the proposed method, we compute the error between the mean of estimated occupancy and the ground truth map, in both cases. Then we sum the absolute value of the error over all voxels in the map as an indicator of map quality. Fig. 6 depicts the evolution of this value over time. As it can be seen from this figure, the proposed method shows less error than the log-odds method, and the difference is growing as more observations are obtained.

Finally, more important than the error reduction is the consistency that the proposed filter offers. This consistency is a very crucial feature for planning purposes. To demonstrate this feature of the proposed method, we first select a subset of voxels at which the error is above a certain threshold. For this set of

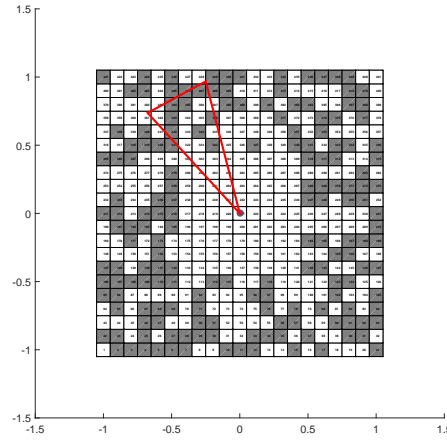


Fig. 2. Ground truth map

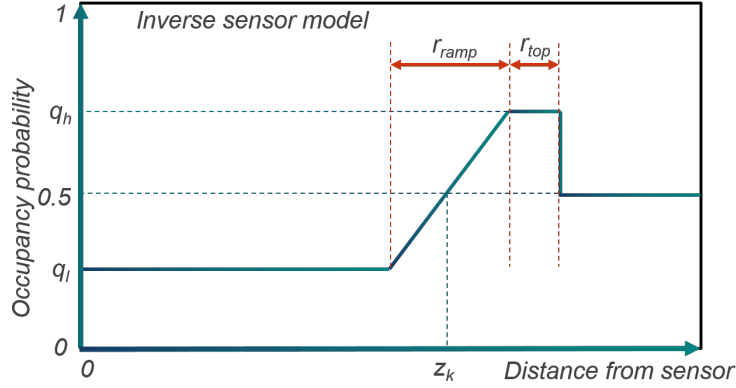


Fig. 3. Inverse sensor model

voxels, Fig. 7 shows the error value (blue) along with the  $2\sigma$  error bound (red). The top axes corresponds to the proposed method and the bottom axes corresponds to the traditional log-odds method.

As it can be seen from top axes in Fig. 7, the  $2\sigma$  bound in the proposed method grows and shrinks in a consistent manner with the error and behaves as a consistent confidence interval that can be used in planning. However, in bottom axes, where log-odds results are shown, there exist many voxels where the error is high (close to -1 or 1, i.e., free has been estimated as fully occupied or vice versa) *at which the variance is very low*, which pose a significant challenge to the planner. In other words, while the large errors are not plausible, the planner can deal with them if the reported variance is high (confidence in the estimated occupancy is low). However, if a high error with low variance (high confidence in wrong estimate) is reported, there are high chances that the planner fails and the robot ends in a collision state.

## VIII. CONCLUSION

This paper proposes a method for joint design of grid-based mapping and planning methods. The mapping algorithm represents occupancy level as a probability distribution that enables the planning

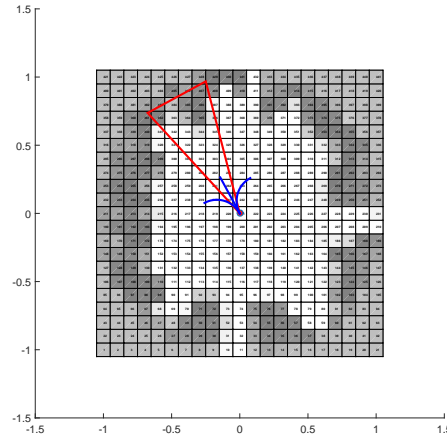


Fig. 4. Map resulted from log-odds method

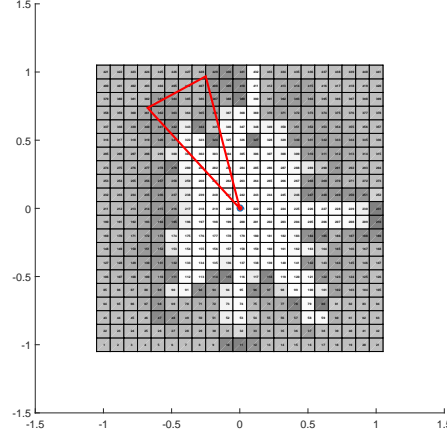


Fig. 5. Map resulted from log-odds method

method to predict the future evolution of the map under different candidate trajectories.

## REFERENCES

- [1] S. Thrun, W. Burgard, and D. Fox, *Probabilistic Robotics*. MIT Press, 2005.
- [2] S. Lavalle and J. Kuffner, “Randomized kinodynamic planning,” *International Journal of Robotics Research*, vol. 20, no. 378-400, 2001.

## IX. APPENDIX

### Cause given observation history:

$$p(c_k | z_{0:k-1}, xv_{0:k}) = \Pr(B^{c_k}, R^{c_k} | z_{0:k-1}, xv_{0:k}) = \Pr(B^{c_k} | z_{0:k-1}, xv_{0:k}) \Pr(R^{c_k} | B^{c_k}, z_{0:k-1}, xv_{0:k})$$

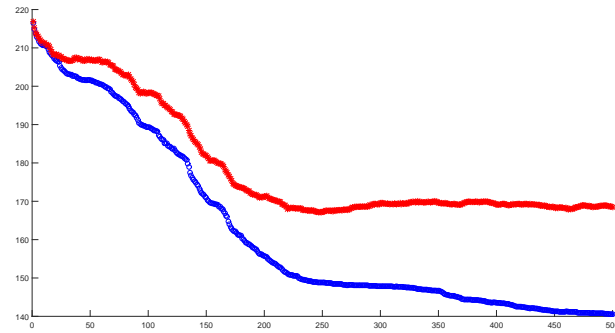


Fig. 6. Full map error evolution over time: comparison between log-odds and the proposed method

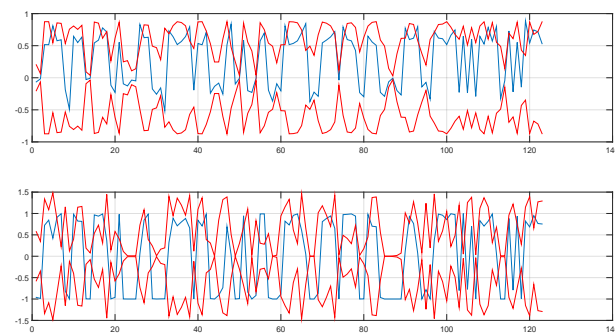


Fig. 7. Mean (blue) and variance ( $3\sigma$  confidence bound – in red) of the mapping error over a set of voxels. Top axes correspond to the proposed method and the bottom axes correspond to the log-odds method.